electronics

Article

An Optimized Multi-Level Control Method for Wireless Power Transfer System Using the Particle Swarm Optimization Algorithm

Jianwei Zhao [1,2], Lin Li [2], Huan Wu [3,*], Bo Luo [3], Huayi Li [1], Yucai Zhang [2], Shanzong Liu [2] and Lei Zhao [2]

[1] Research Center of Satellite Technology, Harbin Institute of Technology, Harbin 150080, China; 21b918143@stu.hit.edu.cn (J.Z.); lihuayi@hit.edu.cn (H.L.)
[2] Shandong Astronautics Electronic Technology Institute, Yantai 264670, China
[3] Yantai Research Institute, Harbin Engineering University, Yantai 264000, China; boluo@hrbeu.edu.cn
* Correspondence: 2335945399wuhuan@hrbeu.edu.cn

Abstract: A Wireless Power Transfer (WPT) system, known for its contactless power delivery, is extensively used for power supply in spacecraft applications. Achieving efficient and stable power transfer necessitates the integration of DC/DC converters on both the primary and secondary sides of WPT systems for power conversion and control. Traditional efficiency optimization methods primarily focus on impedance matching within the wireless power resonance network, often neglecting the overall efficiency optimization of multi-stage DC-DC and WPT systems. This oversight results in suboptimal overall system efficiency despite optimal efficiency in the wireless transmission segment. Additionally, the time-varying nature of mutual inductance and load parameters during power transmission in WPT systems presents challenges for maximum efficiency tracking and power control. This paper introduces a multi-level coordinated control efficiency optimization method for WPT systems utilizing the particle swarm optimization (PSO) algorithm. This method takes into account the transmission losses across all power conversion units within the WPT system, establishing a mathematical model for the joint optimization of overall system transmission efficiency and power. The PSO algorithm is then employed to solve this optimization model using estimated mutual inductance and load values. By adjusting the DC/DC converters on both sides, the method ensures optimal overall system efficiency and consistent power transmission. Experimental results indicate that under varying load and mutual inductance conditions, a Series–Series (SS) compensated WPT system using this method achieves a 200 W power output with maximum efficiency tracking, a power output error of 0.63%, and an average transmission efficiency of 86.2%. This demonstrates superior power transmission stability and higher efficiency compared to traditional impedance matching methods.

Keywords: multi-level control method; particle swarm optimization (PSO); wireless power transfer (WPT)

Citation: Zhao, J.; Li, L.; Wu, H.; Luo, B.; Li, H.; Zhang, Y.; Liu, S.; Zhao, L. An Optimized Multi-Level Control Method for Wireless Power Transfer System Using the Particle Swarm Optimization Algorithm. *Electronics* **2024**, *13*, 4341. https://doi.org/10.3390/electronics13224341

Academic Editor: Christos J. Bouras

Received: 18 September 2024
Revised: 22 October 2024
Accepted: 30 October 2024
Published: 5 November 2024

1. Introduction

Spacecraft are crucial tools for humanity's exploration of the unknown universe. In deep space, spacecraft primarily convert solar energy into electricity to power onboard equipment, with excess energy stored in batteries [1]. When sunlight is scarce and battery storage is insufficient, spacecraft must obtain energy replenishment from other spacecraft via docking systems [2,3].

Traditional power transfer during spacecraft docking relies on cable connections, a process that is complex and requires high docking precision. Furthermore, docking plugs are subject to mechanical wear and aging, leading to high maintenance costs [4]. Wireless Power Transfer (WPT), a contactless power transmission method [5–7], offers flexibility, efficiency, safety, and reliability [8]. It eliminates the need for direct mechanical contact

and allows for docking misalignment [9], providing a novel solution to spacecraft power supply challenges [10–12].

Transmission efficiency is a key performance metric for WPT systems, particularly in spacecraft where energy acquisition is difficult. Current methods to enhance WPT efficiency focus on optimizing coupling mechanisms and achieving optimal impedance matching [13]. Improving the quality factor of magnetic coupling coils or the coupling system can significantly boost the WPT efficiency. Wire diameter distribution, inner-to-outer diameter ratios, and spatial layouts are optimized to improve coil quality factors and transmission efficiency [14–16]. Advanced materials like nanocrystals and metamaterials have also been used to enhance coupling coil efficiency [17–19]. Additionally, three-coil coupling models have been proposed to increase system efficiency by adding relay coils [20,21]. However, these methods involve complex coil design processes and expensive new materials.

Impedance matching can be categorized into passive and active methods. Passive impedance matching adjusts passive components such as variable capacitors or inductors in the WPT system's resonant network. Ref. [22] has achieved maximum efficiency tracking by switching primary-side passive component networks to maintain optimal operating frequency. Ref. [23] achieved maximum efficiency tracking of the system by adding an inductive network, enhancing the wireless power transmission efficiency of implanted biomedical devices to 58%. Refs. [24,25] achieved maximum efficiency tracking by switching resonant capacitor networks to track the optimal impedance matching point, improving the transmission efficiency of the WPT systems to 88% and 70%, respectively. The active impedance matching method achieves maximum efficiency tracking by adjusting the secondary-side DC/DC converter to match the load resistance with the load point of maximum transmission efficiency. Ref. [26] uses a secondary-side Boost–Buck converter as the impedance matching converter to achieve maximum efficiency tracking, and, in experiments, it can achieve a total system efficiency of over 70%. Ref. [27] introduced a maximum efficiency tracking method using a bilateral DC/DC converter, where the secondary converter tracks maximum efficiency and the primary maintains constant output voltage. This approach enhances overall efficiency across various coupling coefficients and load resistances. Refs. [28,29] presented a method based on dynamic coupling coefficient estimation, relying solely on the inherent tracking circuit, allowing for wide variations in coupling and load while ensuring output controllability. Refs. [30,31] have converted maximum efficiency point tracking into minimum power input point tracking, achieving voltage-regulated maximum efficiency tracking without bilateral communication.

However, these methods primarily focus on the maximum efficiency transfer of the WPT resonant network and do not consider the overall transmission efficiency of WPT systems with multiple power conversion units. The time-varying nature of mutual inductance and load parameters during operation also poses challenges for maximum efficiency tracking and power control.

This paper presents a multi-level control efficiency optimization method for WPT systems based on the particle swarm optimization (PSO) algorithm. This method accounts for the transmission losses of each power conversion unit in the WPT system, constructing a comprehensive multi-level transmission power-efficiency joint optimization model. By using the PSO algorithm to solve the joint optimization model online, the method dynamically adjusts the dual-side DC/DC converters, achieving optimal overall system efficiency and constant power transmission in WPT systems. The main contributions of this article are as follows:

(1) Compared to traditional impedance matching methods for resonant networks, this paper takes into account the transmission losses at various stages of the multi-level WPT system, including the DC-DC converter, which enables more stable power output and higher transmission efficiency.
(2) Considering the variations in load and mutual coupling of the WPT system under different industrial conditions, a joint optimization objective function for power and

efficiency is established, and the PSO algorithm is used for real-time solving, enabling constant power transmission and maximum efficiency in dynamic conditions.

(3) The method used in this paper has good extended applicability and can be applied to various topologies of WPT systems, such as LCC-LCC and LCC-S.

(4) This paper also establishes a 200 W wireless power transmission system to verify the effectiveness of the proposed method.

2. Analysis of the Circuit Model for Multi-Level Cascaded WPT Systems

The WPT system comprises several power conversion units, including a DC power supply, an inverter, a resonant network, and a rectifier. For stable and efficient wireless power transfer, DC/DC converters are incorporated on both sides of the WPT system. The overall structure of the multi-level DC-DC converter WPT system is illustrated in Figure 1. U_{in} denotes the voltage of the DC power supply, U_{inv} denotes the DC voltage at the inverter input, U_{buck} denotes the DC voltage at the Buck converter input, and U_{load} denotes the DC voltage across the load resistor. v_p indicates the AC voltage at the input of the primary side of the resonant network, and v_s indicates the AC voltage at the output of the secondary side of the resonant network. R_{buck} represents the equivalent input resistance of the Buck converter, R_{rec} represents the equivalent input resistance of the rectifier, R_{ss} represents the equivalent input resistance of the Series–Series (SS) resonant compensation network, and R_{inv} represents the equivalent input resistance of the inverter.

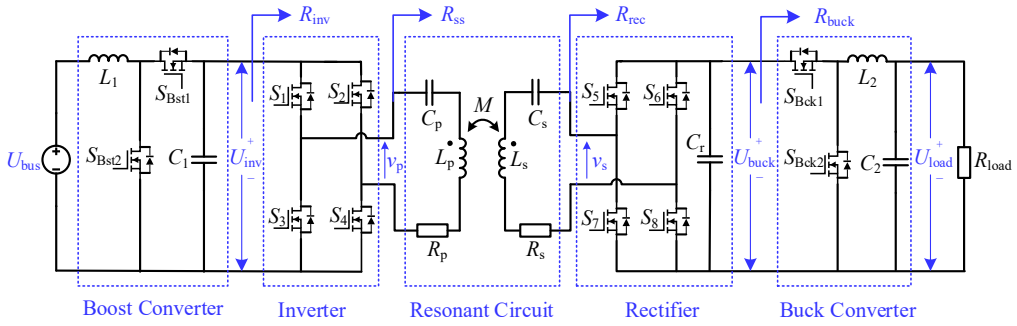

Figure 1. Circuit diagram of the multi-level DC-DC converter WPT system.

2.1. Circuit Analysis for SS Compensated Topology

The equivalent circuit of the SS compensated topology is depicted in Figure 2. C_p and C_s are the compensation capacitors on the primary and secondary sides, respectively. L_p and L_s denote the inductances of the transmitting and receiving coils, respectively, while R_p and R_s indicate the internal resistances of the transmitting and receiving coils. M represents the mutual inductance between the transmitting and receiving coils. v_{p1} is the fundamental component of the AC input voltage v_p. i_{p1} and i_{s1} are the currents in the primary and secondary circuits, with their RMS values indicated as I_p and I_s, respectively. ω is the angular frequency at which the resonant circuit operates.

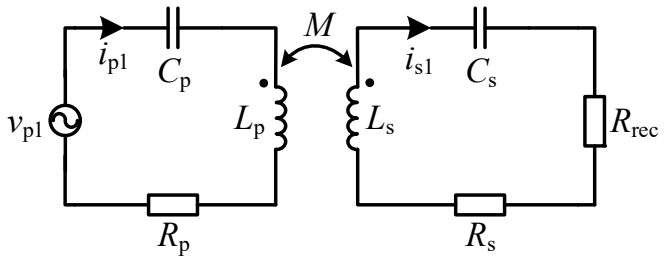

Figure 2. Equivalent system with the SS compensated circuit.

The Kirchhoff's Voltage Law (KVL) equations for the SS compensated resonant network are provided in Equation (1).

$$\begin{cases} v_{p1} = i_{p1} \times \left(\frac{1}{j\omega C_p} + j\omega L_p + R_p\right) - i_{s1} \times j\omega M, \\ 0 = i_{s1} \times \left(j\omega L_s + \frac{1}{j\omega C_s} + R_{rec} + R_s\right) - i_{p1} \times j\omega M. \end{cases} \quad (1)$$

Then, the AC currents i_{p1} and i_{s1} are calculated according to Equation (2).

$$\begin{cases} i_{p1} = \frac{(R_{rec}+R_s+\frac{1}{j\omega C_s}+j\omega L_s)\times v_{p1}}{\omega^2M^2+(R_p+\frac{1}{j\omega C_p}+j\omega L_p)\times(R_{rec}+R_s+\frac{1}{j\omega C_s}+j\omega L_s)}, \\ i_{s1} = \frac{j\omega M\times v_{p1}}{\omega^2M^2+(R_p+\frac{1}{j\omega C_p}+j\omega L_p)\times(R_{rec}+R_s+\frac{1}{j\omega C_s}+j\omega L_s)}, \end{cases} \quad (2)$$

when the primary and secondary sides of the system are in resonance, where $j\omega L_p + 1/j\omega C_p = 0$ and $j\omega L_s + 1/j\omega C_s = 0$, the currents i_{p1} and i_{s1} can be obtained by substituting into Equation (2), as shown in Equation (3).

$$\begin{cases} i_{p1} = \frac{(R_{rec}+R_s)\times v_{p1}}{\omega^2M^2+R_p\times(R_{rec}+R_s)}, \\ i_{s1} = \frac{j\omega M\times v_{p1}}{\omega^2M^2+R_p\times(R_{rec}+R_s)}. \end{cases} \quad (3)$$

The transfer efficiency η_{ss} of the SS resonant network is given by Equation (4).

$$\eta_{ss} = \frac{I_s^2 R_{rec}}{I_s^2 R_{rec} + I_p^2 R_p + I_s^2 R_s} = \frac{\omega^2 M^2 R_{rec}}{(R_{rec}+R_s)^2 R_p + \omega^2 M^2 (Rrec + R_s)}. \quad (4)$$

According to Equation (4), the relationship between the efficiency η_{ss}, the load resistance R_{rec}, and the mutual inductance M is depicted in Figure 3 with the specified parameters. As shown in Figure 3, there is an optimal load resistance, $R_{rec\text{-}max}$, that maximizes the efficiency of the resonant network. Additionally, the transmission efficiency improves with an increase in mutual inductance M.

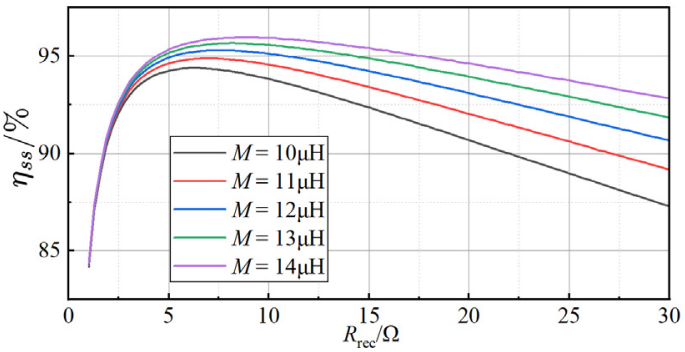

Figure 3. The relationship between the efficiency η_{ss}, load resistance R_{rec}, and mutual inductance M (where operating frequency f = 100 kHz, R_p = 181.5 mΩ, R_S = 181.53 mΩ).

2.2. Analysis of Losses in the Boost Converter

The circuit diagram of the Boost converter is illustrated in Figure 4. It employs two GaN power switches controlled synchronously to minimize transmission losses. S_{Bst1} and S_{Bst2} are GaN power switches, with R_{on} denoting their on-resistance. L_1 is the inductor in the converter, with R_{L1} representing its series resistance. i_{L1} is the current flowing through the inductor, and v_{L1} is the voltage across it. C_1 is the capacitor in the converter, with i_{C1} representing the current through the capacitor, and $u_1(t)$ is the output voltage. The duty cycle of the Boost converter is denoted by d_1.

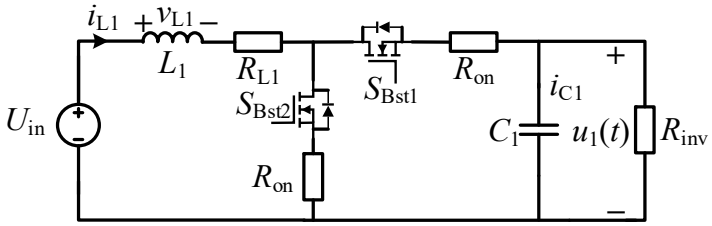

Figure 4. Schematic diagram of the Boost converter.

Taking into account the inductor losses and the conduction losses of the GaN power switches in the Boost converter, the following relationships are present within a switching period T_s:

$$\begin{cases} v_{L1}(t) = \begin{cases} U_{in} - i_{L1}(t) \times (R_{on} + R_{L1}), 0 < t < d_1 T_s, \\ U_{in} - i_{L1}(t) \times (R_{on} + R_{L1}) - u_1(t), d_1 T_s < t < T_s. \end{cases} \\ i_{C1}(t) = \begin{cases} -u_1(t)/R_{inv}, 0 < t < d_1 T_s, \\ i_{L1}(t) - u_1(t)/R_{inv}, d_1 T_s < t < T_s. \end{cases} \end{cases} \tag{5}$$

Based on the principles of volt-second and ampere-second balance, the following equations are derived:

$$\begin{cases} \int_0^{d_1 T_s} v_{L1}(t)dt + \int_{d_1 T}^{T_s} v_{L1}(t)dt = 0, \\ \int_0^{d_1 T_s} i_{C1}(t)dt + \int_{d_1 T}^{T_s} i_{C1}(t)dt = 0. \end{cases} \tag{6}$$

The results of the calculations are given in Equation (7). Using this equation, the simplified circuit diagram of the system is shown in Figure 5:

$$\begin{cases} U_{in} - I_{L1}(R_{on} + R_{L1}) = (1 - d_1)U_{inv}, \\ (1 - d_1)I_{L1} = U_{inv}/R_{inv}. \end{cases} \tag{7}$$

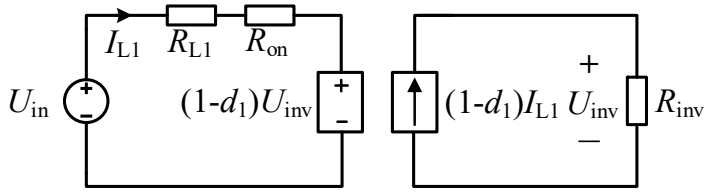

Figure 5. Simplified schematic diagram of the Boost converter.

Further, the transmission efficiency of the Boost converter is determined by Equation (8).

$$\eta_{boost} = \frac{(1 - d_1)^2 R_{inv}}{(1 - d_1)^2 R_{inv} + R_{L1} + R_{on}}. \tag{8}$$

According to Equation (8), the efficiency of the Boost converter, considering switch and inductor losses, is compared under various duty cycles d_1 and load conditions, as shown in Figure 6. Figure 6 indicates that the Boost converter's efficiency η_{boost} increases with the load resistance R_{inv} and decreases with a higher duty cycle d_1.

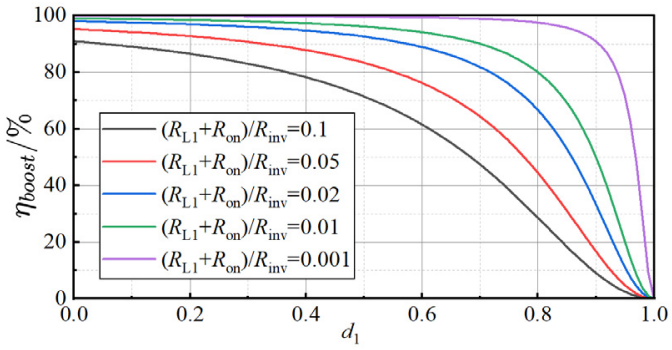

Figure 6. The relationship between η_{boost}, d_1, and R_{inv}. (f_s = 100 kHz, R_{L1} =11 mΩ, and R_{on} = 10 mΩ).

2.3. Analysis of Losses in the Buck Converter

The circuit diagram of the Buck converter is shown in Figure 7. It utilizes a synchronous control scheme similar to the Boost converter. S_{Bck1} and S_{Bck2} are GaN power switches, with Ron indicating their on-resistance. L_2 is the inductor in the converter, with R_{L2} representing its series resistance. i_{L2} is the current through the inductor, and v_{L2} is the voltage across it. C_2 is the capacitor in the converter, with i_{C2} representing the current through it, and $u_2(t)$ is the output voltage. The duty cycle of the Buck converter is represented by d_2.

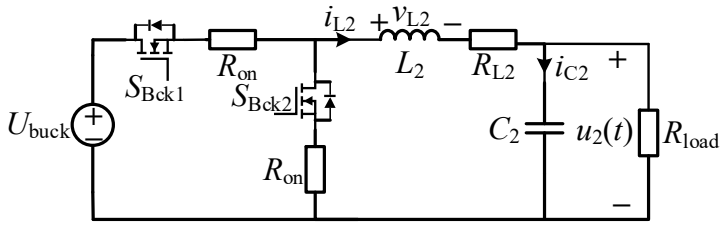

Figure 7. Schematic diagram of the Buck converter.

Taking into account the on-resistance of the GaN power switches and the inductor resistance R_{L2}, the following relationships hold within a switching period T_s:

$$\begin{cases} v_{L1}(t) = \begin{cases} U_{buck} - i_{L2}(t)(R_{on} + R_{L2}) - u_2(t), 0 < t < d_2T_s, \\ -i_{L2}(t)(R_{on} + R_{L2}) - u_2(t), d_2T_s < t < T_s. \end{cases} \\ i_{C1}(t) = i_{L2}(t) - u_2(t)/R_{load}. \end{cases} \tag{9}$$

According to the principles of volt-second and ampere-second balance, the following equations are derived:

$$\begin{cases} \int_0^{d_2T_s} v_{L2}(t)dt + \int_{d_2T_s}^{T_s} v_{L2}(t)dt = 0, \\ \int_0^{d_2T_s} i_{C2}(t)dt + \int_{d_2T_s}^{T_s} i_{C2}(t)dt = 0. \end{cases} \tag{10}$$

The results of the calculations are provided in Equation (11). Using this equation, the simplified circuit diagram of the system is shown in Figure 8.

$$\begin{cases} d_2U_{buck} = I_{L2}(R_{on} + R_{L2}) + U_{load}, \\ I_{L2} = U_{load}/R_{load}. \end{cases} \tag{11}$$

The transmission efficiency of the Buck converter is expressed by Equation (12):

$$\eta_{buck} = \frac{R_{load}}{R_{load} + R_{on} + R_{L2}}. \tag{12}$$

Based on Equation (12), in a synchronous control scheme where only conduction and inductor losses are considered, the transmission efficiency of the Buck converter is influenced solely by the load resistance R_{load} and is independent of the duty cycle d_2.

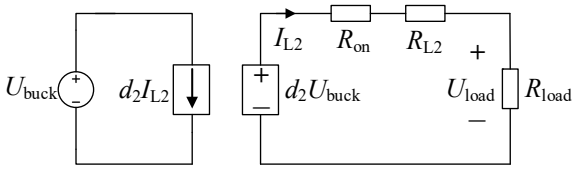

Figure 8. Simplified schematic diagram of the Buck converter.

3. Analysis of Overall Transmission Efficiency and Power in Multi-Stage Controlled WPT Systems

3.1. Analysis of Overall Transmission Efficiency in WPT Systems

As illustrated in Figure 1, the overall transmission efficiency η of the multi-stage controlled WPT system is determined by the efficiencies of each stage of energy conversion. The expression for this efficiency is given by $\eta = \eta_{buck} \times \eta_{ss} \times \eta_{boost}$, considering that the losses in the rectifier bridge and inverter are relatively fixed and independent of d_1 and d_2. Thus, the overall transmission efficiency η is a function of the duty cycles d_1 and d_2 of the primary-side Buck converter and Boost converter, as represented in Equation (13).

$$\eta = f(d_1, d_2) = \frac{\omega^2 M^2 R_{rec}}{(R_{rec} + R_s)^2 R_p + \omega^2 M^2 (R_{rec} + R_s)} \times \frac{1}{1 + \frac{R_{on} + R_{L2}}{R_{load}}} \times \frac{1}{1 + \frac{R_{L1} + R_{on}}{(1-d_1)^2 R_{inv}}}. \tag{13}$$

The expressions for the equivalent loads R_{inv} and R_{rec} are provided in Equation (14).

$$\begin{cases} R_{rec} = \frac{8}{\pi^2} R_{buck} = \frac{8}{\pi^2} \frac{R_{on} + R_{L2} + R_{load}}{d_2^2}, \\ R_{inv} = \frac{\pi^2}{8} R_{ss} = \frac{\pi^2}{8} (R_p + \frac{\omega^2 M^2}{R_s + R_{rec}}). \end{cases} \tag{14}$$

According to Equations (13) and (14), Figure 9 illustrates how the transmission efficiency η of the WPT system changes as a function of d_1 and d_2.

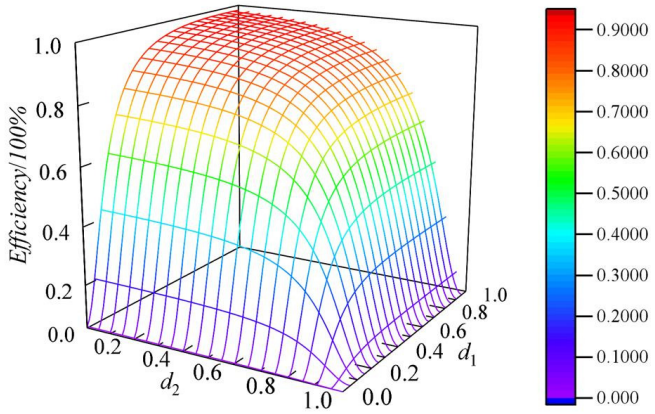

Figure 9. The relationship between the transmission efficiency of the multi-stage WPT system and the duty cycles d_1 and d_2. Parameters are set as follows: f_s = 100 kHz, M = 12.62 µH, R_{L1} = 11 mΩ, R_{on} = 10 mΩ, R_{L2} = 12 mΩ, R_p = 181.5 mΩ, and R_s = 181.53 mΩ.

As shown in Figure 9, the overall transmission efficiency of the multi-stage WPT system is influenced by both the duty cycles d_1 and d_2. This indicates that traditional maximum efficiency tracking methods based solely on resonant network impedance matching are limited in their effectiveness.

3.2. Analysis of Transfer Power in Multi-Stage Controlled WPT Systems

The load power P in the multi-stage WPT system is determined by the duty cycles d_1 and d_2 of the primary-side Boost converter and secondary-side Buck converter, as expressed in Equation (15):

$$P = g(d_1, d_2) = \frac{U_{\text{load}}^2}{R_{\text{load}}}. \tag{15}$$

The calculation of U_{load} is detailed in Equation (16), with the expressions for R_{inv} and R_{rec} given in Equation (14):

$$\begin{cases} U_{\text{inv}} = \frac{(1-d_1)R_{\text{inv}}}{R_{L1}+R_{\text{on}}+(1-d_1)^2\times R_{\text{inv}}}U_{\text{in}}, \\ U_{\text{buck}} = \frac{\omega M R_{\text{rec}}}{\omega M^2+R_p\times(R_{\text{inv}}+R_s)}U_{\text{inv}}, \\ U_{\text{load}} = \frac{d_2\times R_{\text{load}}}{R_{\text{on}}+R_{\text{L2}}+R_{\text{load}}}U_{\text{buck}}. \end{cases} \tag{16}$$

The intersection of the space surfaces representing the rated load power $P(d_1,d_2) = P_{set}$ and the transmission efficiency $\eta(d_1,d_2)$ of the multi-stage WPT system, as calculated from Equations (15) and (16), is depicted.

In Figure 10, the red surface represents the constraint of the rated transmission power P_{set}. The intersection of the red surface with the transmission efficiency surface indicates the system's transmission efficiency when the load power is set to P_{set}. At this intersection line, there is a maximum value max, where the WPT system achieves its highest transmission efficiency while meeting the rated power P_{set}.

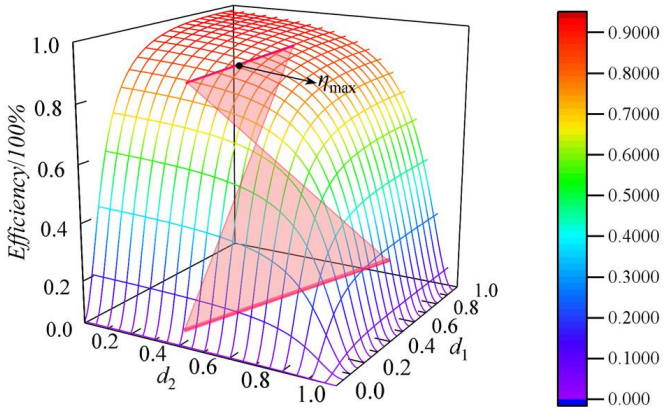

Figure 10. The relationships between the efficiency, d_1 and d_2. (U_{in} = 28 V, f_s = 100 kHz, M = 12.62 uH, R_{L1} = 11 mΩ, R_{on} = 10 mΩ, R_{L2} = 12 mΩ, R_p = 181.5 mΩ, R_s = 181.53 mΩ, and R_{load} = 8Ω).

4. Efficiency Optimization Method Using Particle Swarm Optimization Algorithm

4.1. Formulation of the Objective Function

Directly solving for the duty cycles d_1 and d_2 that ensure maximum efficiency tracking and constant power transmission using Equations (14) and (16) is challenging, especially under conditions with time-varying parameters. The system requires the continuous adjustment of d_1 and d_2. To address this, this paper proposes an approach that involves constructing an optimization model and solving it in real time to achieve efficient and stable power transmission under varying conditions.

The objective function $J(\boldsymbol{d})$ is constructed based on the multi-stage efficiency and power optimization goals of the WPT system, as follows:

$$J(\boldsymbol{d}) = \lambda_1[1-\eta(d_1,d_2)]^2 + \lambda_2[P_{set}-P(d_1,d_2)]^2. \tag{17}$$

In Equation (17), P_{set} denotes the specified rated load power, while the duty cycles d_1 of the Boost converter on the transmitter side and d_2 of the Buck converter on the

receiver side constitute the decision variable matrix $\boldsymbol{d} = [d_1, d_2]^{\mathrm{T}}$. λ_1 and λ_2 are the linear weighting coefficients of the objective function $J(\boldsymbol{d})$, with their sum equaling to 1. A larger λ_1 emphasizes optimization towards maximizing transmission efficiency, whereas a larger λ_2 prioritizes stable power transmission.

Thus, the mathematical model for the combined optimization of the WPT system's overall transmission efficiency and power is formulated as shown in Equation (18). The solution to this optimization equation represents the point of maximum efficiency in the multi-stage WPT system.

$$\begin{cases} \min J(\boldsymbol{d}) = \lambda_1(1-\eta)^2 + \lambda_2(P_{set}-P)^2, \\ \boldsymbol{d} = [d_1, d_2]^{\mathrm{T}}, \\ \text{s.t.} \begin{cases} \sum\limits_{i=1}^{2} \lambda_i = 1, \\ 0 \le d_1 \le 1, \\ 0 \le d_2 \le 1. \end{cases} \end{cases} \tag{18}$$

4.2. Maximum Efficiency Tracking Using Particle Swarm Optimization Algorithm

When a system operates under conditions where parameters vary over time, traditional optimization algorithms may struggle to meet speed and efficiency requirements. In contrast, the PSO algorithm [31,32], known for its simplicity and rapid convergence, is widely used for solving optimization problems. By employing PSO, it is possible to significantly enhance the dynamic performance of the system and achieve optimal efficiency tracking and power control in WPT systems under varying parameter conditions.

The PSO algorithm relies on the concepts of population and fitness. It operates by having each particle in the population interact with others and share information to find the optimal solution to the objective function. In the context of the joint optimization model for WPT system transmission efficiency and power presented in this paper, each particle represents a set of duty cycle matrices d = $[d_1, d_2]^{\mathrm{T}}$. A population of such particles is used, with each particle's fitness calculated based on the objective function $J(\boldsymbol{d})$. Through iterative updates and refinements, the optimal duty cycle matrix d is determined.

The method for solving the WPT system transmission power-efficiency joint optimization model using PSO is outlined in Equation (19).

$$\begin{cases} \boldsymbol{v}_{(i,n+1)} = w\boldsymbol{v}_{(i,n+1)} + c_1 r_1 \left(\boldsymbol{d}_{pbest,i} - \boldsymbol{d}_{(i,n)} \right) + c_2 r_2 \left(\boldsymbol{d}_{gbest} - \boldsymbol{d}_{(i,n)} \right), \\ \boldsymbol{d}_{(i,n+1)} = \boldsymbol{d}_{(i,n)} + \boldsymbol{v}_{(i,n+1)}. \end{cases} \tag{19}$$

In the PSO algorithm, $d_{(\mathrm{i,n})}$ and $v_{(\mathrm{i,n})}$ represent the position and velocity of the i-th particle at the n-th iteration, respectively. $\boldsymbol{d}_{\mathrm{pbest,i}}$ denotes the best fitness position found by the i-th particle from the start up to the n-th iteration, known as the individual best position. $\boldsymbol{d}_{\mathrm{gbest}}$ is the best fitness position found by any particle from the start up to the n-th iteration, known as the global best position. The inertia weight is denoted by w, r_1, and r_2 are random numbers uniformly distributed between 0 and 1, and c_1 and c_2 are the individual and social learning factors, respectively.

The PSO algorithm may experience premature convergence and become trapped in local optima. Expanding the population size and increasing the number of iterations can slow down the convergence process. To address this issue, an inertia weight decay strategy is introduced to enhance the search capability of the PSO algorithm, as described in Equation (20).

$$w = w_{\max} - \frac{(w_{\max} - w_{\min})n^2}{N^2}. \tag{20}$$

where N denotes the maximum number of iterations, $w_{\max}$ is the maximum inertia weight, and $w_{\min}$ is the minimum inertia weight.

The flowchart for solving the power-efficiency joint optimization model of the multi-stage WPT system using the PSO algorithm is illustrated in Figure 11.

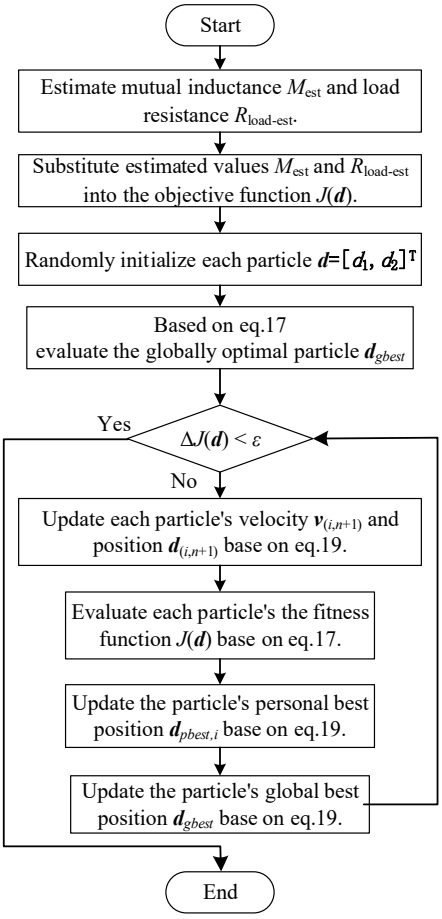

Figure 11. System optimization process based on PSO algorithm.

5. Experimental Validation

To validate the effectiveness of the proposed method, an experimental platform was constructed, as shown in Figure 12. The platform primarily consists of a DC power supply, an inverter, SS resonant compensation capacitors, coupling coils, a rectifier bridge, an electronic load, Buck and Boost DC-DC converters, and a wireless communication module.

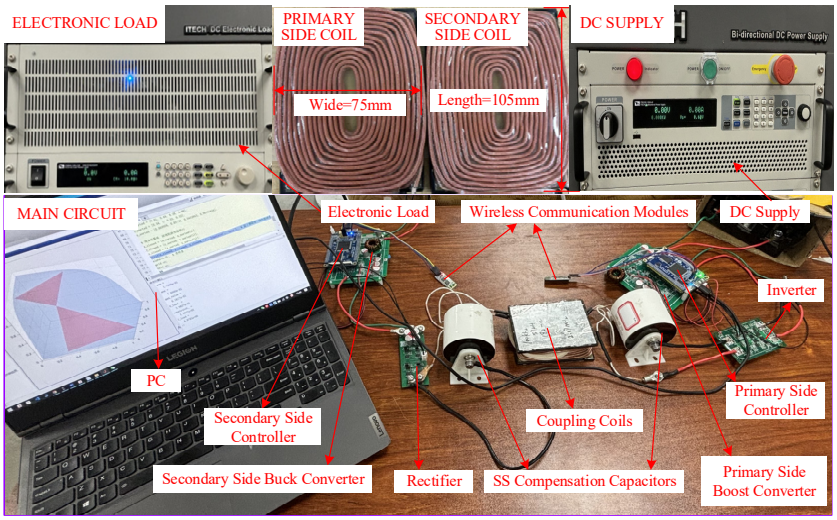

Figure 12. Physical image of the experimental platform.

As depicted in Figure 12, both the transmitter and receiver coils are wound from Litz wire, each consisting of 2 layers with 12 turns. The mutual coupling between the coils can be adjusted by modifying their relative positions. A constant voltage DC power supply is used, and a programmable DC electronic load serves as the output load. GaN power switches are employed in the Buck and Boost converters, as well as in the inverter and rectifier bridge. The WPT system's primary and secondary sides both utilize STM32F407 microcontrollers to provide drive and control signals for the GaN power switches. Additional parameters of the experimental platform components are listed in Table 1.

Table 1. Specific parameters of the experimental platform.

Parameter	Physical Meaning	Value
f	Resonant frequency	100 kHz
U_{in}	DC input voltage	28.0 V
L_1	Inductance of the Boost converter	30.0 uH
C_1	Capacitance of the Boost converter	200 uF
R_{L1}	Resistance of the Boost inductor	42 mΩ
Cp	Primary-side resonant capacitor	43.6 nF
Lp	Primary-side coil inductance	58.0 uH
R_{Lp}	Series resistance of the primary coil	243 mΩ
C_s	Secondary-side resonant capacitor	43.6 nF
L_s	Secondary-side coil inductance	58.0 uH
R_{Ls}	Resistance of the secondary coil	242 mΩ
L_2	Inductance of the Buck converter	30.0 uH
R_{L2}	Resistance of the Buck inductor	18 mΩ
R_{on}	On-resistance of switches	11 mΩ

Figure 13 shows the schematic diagram of maximum efficiency tracking for the WPT system using the PSO algorithm. The process begins with estimating the load resistance $R_{\text{load-est}}$ using the load voltage U_{load} and current I_{load} based on Equation (21). Next, the mutual inductance Mest is estimated from the effective currents I_s and I_p of the SS resonant network. Using the estimated load resistance $R_{\text{load-est}}$ and mutual inductance Mest, these values are substituted into the power-efficiency joint optimization function. PSO is then applied to determine and adjust the duty cycles $\boldsymbol{d} = [d_1, d_2]^{\mathrm{T}}$ of the Buck and Boost converters to achieve constant power transmission and maximize efficiency in the multi-stage WPT system.

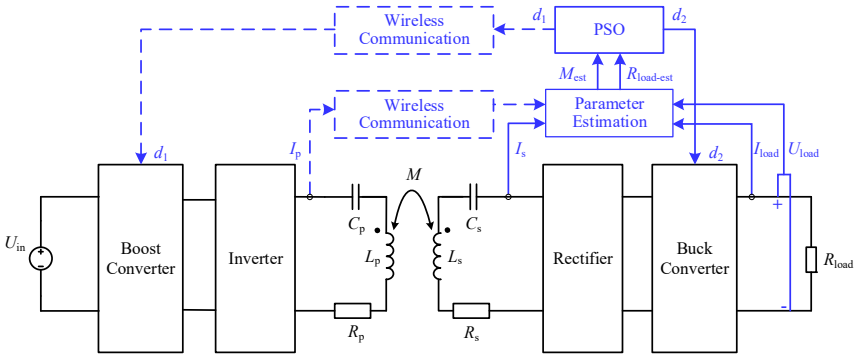

Figure 13. Principle diagram of multi-level joint efficiency optimization for WPT system using PSO algorithm.

5.1. Load Estimation Experiment

When the load consists of energy storage components such as lithium batteries or supercapacitors, the load model parameters can change with the charging time of the battery. Therefore, to enhance the transmission efficiency and stability of the WPT system, this study estimates the load resistance R_{load} using the load voltage U_{load} and load current I_{load}. As illustrated in Figure 13, the load estimation formula is as follows.

$$R_{\text{load-est}} = U_{\text{load}} / I_{\text{load}}. \tag{21}$$

In this study, a programmable electronic load is used to simulate the variation in the equivalent resistance of energy storage loads. The programmable electronic load resistance is set to increase sequentially from 3 Ω to 8 Ω. The real and estimated values of the load resistance are listed in the table below. The experiment demonstrates that the average estimation error of the load resistance is 1.65%, indicating a high level of accuracy in the estimation, shown as Table 2.

Table 2. Real and estimated values of load resistance.

No.	R_{load}/Ω	$R_{load\text{-}est}$/Ω	Error
1	3.0	3.09	3.0%
2	4.0	4.10	2.5%
3	5.0	5.02	0.4%
4	6.0	6.11.	1.8%
5	7.0	6.92	1.1%
6	8.0	8.09	1.1%

5.2. Mutual Inductance Estimation Experiment

The WPT system is a loosely coupled system, where misalignment between the primary and secondary coils can easily shift the system away from its optimal operating point. To address this, mutual inductance is estimated by measuring the currents, as illustrated in Figure 13.

According to Equation (22), the ratio of the effective currents on the secondary-side I_s to the primary-side I_p in the SS topology is directly correlated with the mutual inductance M:

$$\frac{I_s}{I_p} = \frac{\omega M}{R_{rec} + R_s}. \tag{22}$$

Therefore, the estimation formula for mutual inductance M_{est} is given by the following:

$$M_{est} = \frac{R_{rec} + R_s}{\omega} \times \frac{I_s}{I_p} = \frac{8R_{on} + 8R_{L2} + 8R_{load\text{-}est} + R_s\pi^2 d_2^2}{\pi^2 d_2^2 \omega} \times \frac{I_s}{I_p}. \tag{23}$$

To simulate the coil displacement, the coupling coil's spatial distance was adjusted, as illustrated in Figure 14. The mutual inductance of the coils was estimated online under the following four conditions: (1) $\Delta x = 0$ cm, $\Delta y = 0$ cm, and $\Delta z = 1$ cm; (2) $\Delta x = 1$ cm, $\Delta y = 0$ cm, and $\Delta z = 1$ cm; (3) $\Delta x = 0$ cm, $\Delta y = 1$ cm, and $\Delta z = 1$ cm; and (4) $\Delta x = 0$ cm, $\Delta y = 0$ cm, and $\Delta z = 2$ cm.

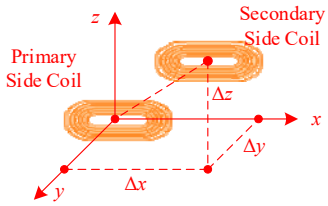

Figure 14. Diagram of coil spatial distance.

By measuring the effective current values I_s and I_p on both sides of the primary and secondary resonant networks, and using Equation (23), the mutual inductance M_{est} of the coupling coils at different spatial distances is calculated. The estimated values are compared with those measured using an impedance analyzer (LCR meter), as shown in Table 3. The experimental results indicate that the average error in estimating the mutual inductance M is 0.27%, demonstrating the high accuracy of the proposed method for estimating the mutual inductance of coupling coils.

Table 3. Mutual inductance values of coupling coils at different spatial distances.

No.	Δ*x*/cm	Δ*y*/cm	Δ*z*/cm	*M*/uH	M_{calc}/uH	Error
1	0	0	1	20.99	20.86	0.6%
2	1	0	1	16.01	15.98	0.2%
3	0	1	1	14.63	14.60	0.2%
4	0	0	2	12.62	12.61	0.08%

5.3. Experimental Verification of the Maximum Efficiency Tracking Based on PSO Algorithm

As shown in Figure 13, the experiment involved using sensors to read the current and voltage values on the load side and the currents on both sides of the resonant network. The primary-side current was transmitted to the secondary side via a wireless communication module. The secondary side's main control chip then estimated the load resistance R_{load} and the mutual inductance M of the coupling coils based on the methods discussed earlier. These estimated values M_{est} and $R_{load\text{-}est}$ were then sent to a PC where MATLAB was used to quickly solve the optimization problem using the PSO algorithm, yielding the optimal duty cycles $\boldsymbol{d} = [d_1, d_2]^T$. The controllers on both the primary and secondary sides adjusted the duty cycles of their respective DC converters according to the optimized values $\boldsymbol{d} = [d_1, d_2]^T$, ensuring that the WPT system achieved rated power transmission and maximum efficiency tracking under varying mutual inductance and load conditions. The parameters for the PSO algorithm are listed in Table 4.

Table 4. PSO algorithm parameter settings.

Parameter	Meaning	Set Value
λ_1	Efficiency weight parameter	0.99
λ_2	Power weight parameter	0.01
N	Maximum number of iterations	100
POP	Population size	100
c_1	Individual learning factor	0.3
c_2	Social learning factor	0.7
w_{max}	Maximum inertia factor	0.5
w_{min}	Minimum inertia factor	0.1

During the experiment, the adaptability of the proposed method to dynamic conditions was verified by adjusting the spatial distance of the WPT system's coupling coils and the resistance value of the electronic load. The experiment followed the following sequential states: (1) coils aligned without offset, M = 20.99 uH, R_{load} = 3 Ω; (2) coils aligned without offset, M = 20.99 uH, R_{load} = 4 Ω; (3) coils offset in the x-direction, M = 16.01 uH, R_{load} = 5 Ω; (4) coils offset in the x-direction, M = 16.01 uH, R_{load} = 6 Ω; (5) coils offset in the y-direction, M = 14.63 uH, R_{load} = 7 Ω; and (6) coils offset in the z-direction, M = 12.62 uH, R_{load} = 8 Ω.

The load voltage and current waveforms obtained using the proposed method and the traditional resonance network impedance matching method are shown in Figures 15 and 16, respectively.

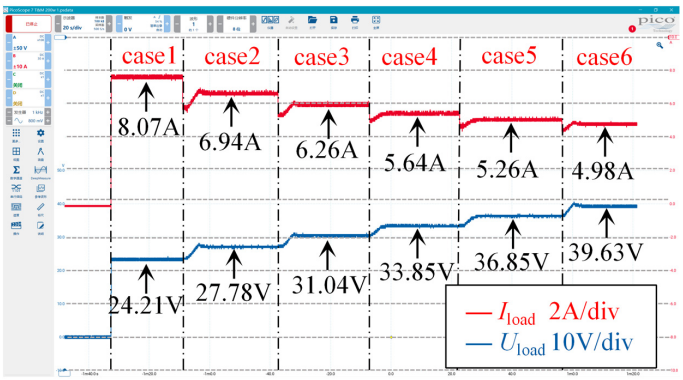

Figure 15. Results from the traditional resonance network impedance matching method.

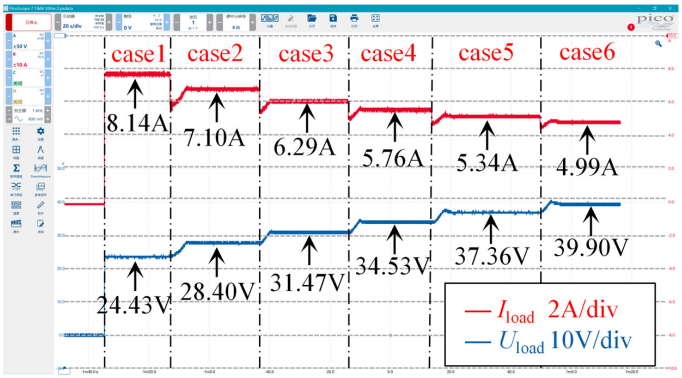

Figure 16. Results from the method proposed in this paper.

A comparison of the experimental results obtained using the traditional resonance network impedance matching method and the method proposed in this paper is shown in Tables 5 and 6. The traditional method yielded an average transmission efficiency η of 80.0% and an average transmission power of 193.55 W. In contrast, the method proposed in this paper achieved an average transmission efficiency of 86.2% and an average transmission power of 199.29 W. Therefore, the proposed method demonstrates more stable power transmission and higher transmission efficiency under dynamic conditions where mutual inductance and load vary.

Table 5. Experimental results of the traditional resonance network impedance matching method.

Case	d_1	d_2	U_{load}/V	I_{load}/A	P/W	η
1	52%	43%	24.21	8.07	195.30	77.6%
2	52%	50%	27.78	6.94	192.79	77.8%
3	45%	63%	31.04	6.26	192.00	80.6%
4	45%	70%	33.85	5.64	190.93	80.7%
5	43%	79%	36.85	5.26	193.97	81.2%
6	39%	90%	39.63	4.98	196.30	82.1%

Table 6. Experimental results of the proposed method.

Case	d_1	d_2	U_{load}/V	I_{load}/A	P/W	η
1	15%	23%	24.43	8.14	198.88	86.2%
2	14%	26%	28.40	7.10	201.62	86.3%
3	13%	38%	31.47	6.29	198.06	86.2%
4	12%	41%	34.53	5.76	198.77	86.3%
5	13%	49%	37.36	5.34	199.45	86.2%
6	12%	60%	39.90	4.99	198.98	86.0%

5.4. Comparative Analysis

The experiments indicate that the traditional method based on resonance network impedance matching fails to achieve maximum efficiency tracking in a multi-stage WPT system and cannot ensure stable transmission of the system's rated power. The method proposed in this paper takes into account the transmission losses in each stage of the WPT system. By employing the PSO algorithm to solve the joint power-efficiency optimization model, the proposed method can achieve consistent 200 W power transmission and overall maximum efficiency tracking under varying conditions. A comparison between the proposed method and the traditional resonance network impedance matching method is illustrated in Figure 17. The experimental results show that the proposed method achieved an average transmission efficiency of 86.20%, which is 6.20% higher than that of the traditional method. Moreover, the power transmission remained stable at around 200 W with an average error of 0.63%, which is lower than the error observed in the traditional method. Therefore, the proposed method offers a significant improvement in achieving stable power

transmission and maximum efficiency tracking in a multi-stage WPT system under different operating conditions compared to the traditional impedance matching method. We conducted a comparison of three algorithms: GA, PSO, and FSO. The experimental results are shown in Table 7, where the PSO algorithm performed the best.

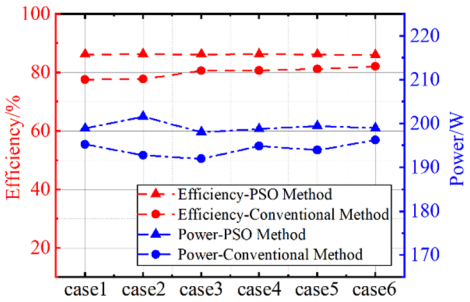

Figure 17. Comparison of experimental results.

Table 7. Comparison of experimental results for GA, FSO, and PSO algorithms.

Algorithm	Case	d_1	d_2	*P*/*W*	η
GA	1	26%	26%	210.59	85.35%
	2	38%	37%	204.5	83.56%
	3	23%	44%	194.98	85.84%
	4	20%	44%	212.08	85.79%
	5	13%	50%	192.73	86.37%
	6	30%	78%	196.57	84.36%
FSO	1	55%	46%	194.26	75.97%
	2	44%	42%	196.50	81.18%
	3	39%	56%	206.03	82.54%
	4	39%	61%	198.73	82.9%%
	5	24%	57%	219.35	83.5%
	6	21%	68%	228.63	84.3%
PSO	1	15%	23%	198.88	86.2%
	2	14%	26%	201.62	86.3%
	3	13%	38%	198.06	86.2%
	4	12%	41%	198.77	86.3%
	5	13%	49%	199.45	86.2%
	6	12%	60%	198.98	86.0%

Based on the above experimental results, the PSO algorithm exhibits a faster convergence speed and has better global search capability. The average power value in six cases is 199.29 W, with an average relative power error of 0.6% and an average efficiency of 86.2%. The GA algorithm has a slower convergence speed and is prone to becoming trapped in local optimal solutions. In six cases, the average power value is 201.9 W, with an average relative power error of 3.57% and an average efficiency of 85.21%. The FSO algorithm is unstable during the initial convergence phase, and, under the same number of iterations, its convergence effect is not as good as that of the PSO and GA algorithms. The average power value in six cases is 207.25 W, with an average relative power error of 5.37% and an average efficiency of 81.73%.

6. Conclusions

This paper proposes a power-efficiency joint optimization method based on the PSO algorithm for power control and maximum efficiency tracking in multi-stage WPT systems. Compared to traditional resonant network impedance matching methods, this approach comprehensively considers the transmission losses at each stage of the multi-stage WPT system, achieving more stable power output and higher transmission efficiency under various operating conditions. Experimental results indicate that the PSO algorithm can

converge within 100 iterations, and, compared to other swarm intelligence optimization algorithms, the results obtained using PSO demonstrate superior performance. The proposed method achieves an average error of only 0.63% at a rated output power of 200 W, with an average transmission efficiency of approximately 86.20%, which is an improvement of 6.20% over traditional methods.

The proposed method is not only applicable to SS resonance network topologies but also extends to various other network topologies such as LCC-S and LCC-LCC. Future research will incorporate the current and voltage parameters of key WPT system components as constraints, ensuring that the system maintains stable power output and maximum efficiency tracking while effectively controlling the overshoot of critical component currents and voltages during the nonlinear variations of mutual inductance and load. This will further enhance the safety and reliability of WPT systems. Meanwhile, future research will consider integrating system identification methods to apply this method to underwater WPT systems, where the model parameters are more significantly affected by the underwater environment, thereby further improving transmission stability and efficiency.

Author Contributions: Conceptualization and Writing—Review and Editing, J.Z.; Methodology, L.L.; Software, H.W.; Validation B.L.; Formal Analysis, H.L.; Data Curation Y.Z.; Visualization S.L.; Supervision, L.Z. All authors have read and agreed to the published version of the manuscript.

Funding: This research received no external funding.

Data Availability Statement: Data are contained within the article.

Conflicts of Interest: The authors declare no conflicts of interest.

References

1. Zhang, J.; Yao, S.; Pan, L.; Bie, Z.; Gao, Z.; Liu, Y.; Zhu, C. Prospects of capacitive power transfer technology in aerospace applications. *Space Electron. Technol.* **2024**, *21*, 1–10.
2. Pothier, N. Spacecraft design considerations for spacecraft charging environments. In Proceedings of the 2017 Asia-Pacific International Symposium on Electromagnetic Compatibility (APEMC), Seoul, Republic of Korea, 20–23 June 2017; IEEE: Piscataway, NJ, USA, 2017; pp. 266–268.
3. Zheng, L.; Zhang, J.; Bie, Z.; Wang, D.; Zhu, C. A Bidirectional Wireless Power Transfer System for Spacecraft Docking Mechanism. In Proceedings of the 2022 IEEE 2nd International Conference on Electronic Technology, Communication and Information (ICETCI), Changchun, China, 27–29 May 2022; IEEE: Piscataway, NJ, USA, 2022; pp. 275–280.
4. Xie, J.; Song, X.; Zhang, Q.; Wang, W. Verification and Improvement of Electric Coupler Plugging in Spacecraft. In Proceedings of the 2020 7th International Forum on Electrical Engineering and Automation (IFEEA), Hefei, China, 25–27 September 2020; IEEE: Piscataway, NJ, USA, 2020; pp. 227–230.
5. Luo, B.; Hu, A.P.; Munir, H.; Zhu, Q.; Mai, R.; He, Z. Compensation Network Design of CPT Systems for Achieving Maximum Power Transfer Under Coupling Voltage Constraints. *IEEE J. Emerg. Sel. Top. Power Electron.* **2022**, *10*, 138–148. [CrossRef]
6. Liu, W.; Luo, B.; He, X.; Wang, Z.; Mai, R. Analysis of compensation topology with constant-voltage/current output for multiple loads capacitive power transfer system. *CSEE J. Power Energy Syst.* **2023**, 1–12. [CrossRef]
7. Zhang, Y.; Luo, B.; Cheng, H.; Wang, Z.; Jiang, C.; Mai, R. A multi-loads capacitive power transfer system for railway intelligent monitoring systems based on single relay plate. *Int. J. Circuit Theory Appl.* **2024**, *52*, 79–96. [CrossRef]
8. Wang, D.; Zhang, J.; Cui, S.; Bie, Z.; Chen, F.; Zhu, C. The state-of-the-arts of underwater wireless power transfer: A comprehensive review and new perspectives. *Renew. Sustain. Energy Rev.* **2024**, *189*, 113910. [CrossRef]
9. Luo, B.; Liu, Y.; Zhang, Y.; Bai, L.; Zhang, Y.; Wang, Z.; You, J.; Mai, R. A Multiple Independent-Load Output Capacitive Power Transfer System with High Coupler Misalignment-Tolerance for Railway Applications. *IEEE Trans. Ind. Appl.* **2024**, *60*, 7566–7577. [CrossRef]
10. Zhang, L.; Song, D.; Zhao, X.; Zhang, Q. Analysis of the development of magnetic field coupled wireless power transfer technology. *Space Electron. Technol.* **2024**, *21*, 11–17.
11. Zhang, L.; Yang, Z.; Zhang, Y.; Zhao, X.; Zhang, Q. Design and verification of micro-nano polymer spacecraft power system based on magnetic coupled wireless power transfer. *Space Electron. Technol.* **2024**, *21*, 79–85.
12. Wang, D.; Cui, S.; Bie, Z.; Zhang, J.; Song, K.; Zhu, C. A Redundancy Design of Wireless Power Transfer System for Satellite Slip Ring with High Reliability. In Proceedings of the 2021 IEEE 4th International Electrical and Energy Conference (CIEEC), Wuhan, China, 28–30 May 2021; IEEE: Piscataway, NJ, USA, 2021; pp. 1–6.
13. Zhang, Z.; Pang, H.; Georgiadis, A.; Cecati, C. Wireless Power Transfer—An Overview. *IEEE Trans. Ind. Electron.* **2019**, *66*, 1044–1058. [CrossRef]

14. Sun, Y.; Liu, X.; Lee, C.K.; Hui, S.Y. On the relationship of quality factor and hollow winding structure of coreless printed spiral winding (CPSW) inductor. *IEEE Trans. Power Electron.* **2012**, *27*, 3050–3056.
15. Cove, S.R.; Ordonez, M.; Shafiei, N.; Zhu, J. Improving Wireless Power Transfer Efficiency Using Hollow Windings with Track-Width-Ratio. *IEEE Trans. Power Electron.* **2016**, *31*, 6524–6533. [CrossRef]
16. Lee, S.H.; Lorenz, R.D. Development and Validation of Model for 95%-Efficiency 220-W Wireless Power Transfer Over a 30-cm Air Gap. *IEEE Trans. Ind. Appl.* **2011**, *47*, 2495–2504. [CrossRef]
17. Yao, C.; Zhang, Y.; Ma, D.; Tang, H. Enhancing the coupling of a two-coil system using a super's caterer. *Int. J. Mod. Phys. B* **2016**, *30*, 1650015. [CrossRef]
18. Chen, C.; Jiang, C.Q.; Ma, T.; Zhang, B.; Xiang, J.; Zhou, J. Core Loss Optimization for Compact Coupler via Square Crushed Nanocrystalline Flake Ribbon Core. *IEEE Trans. Power Electron.* **2024**, *39*, 9095–9099. [CrossRef]
19. Chen, C.; Jiang, C.; Wang, Y.; Fan, Y.; Luo, B.; Cheng, Y. Compact Curved Coupler with Novel Flexible Nanocrystalline Flake Ribbon Core for Autonomous Underwater Vehicles. *IEEE Trans. Power Electron.* **2024**, *39*, 53–57. [CrossRef]
20. Zhong, W.X.; Zhang, C.; Liu, X.; Hui, S.Y.R. A Methodology for Making a Three-Coil Wireless Power Transfer System More Energy Efficient Than a Two-Coil Counterpart for Extended Transfer Distance. *IEEE Trans. Power Electron.* **2015**, *30*, 933–942. [CrossRef]
21. Ye, Z.; Sun, Y.; Dai, X.; Tang, C.; Wang, Z.; Su, Y. Energy Efficiency Analysis of U-coil Wireless Power Transfer System. *IEEE Trans. Power Electron.* **2015**, *31*, 4809–4817. [CrossRef]
22. Beh, T.C.; Imura, T.; Kato, M.; Hori, Y. Basic study of improving efficiency of wireless power transfer via magnetic resonance coupling based on impedance matching. In Proceedings of the 2010 IEEE International Symposium on Industrial Electronics, Bari, Italy, 4–7 July 2010; IEEE: Piscataway, NJ, USA, 2010; pp. 2011–2016.
23. Xue, R.; Cheng, K.; Je, M. High-Efficiency Wireless Power Transfer for Biomedical Implants by Optimal Resonant Load Transformation. *IEEE Trans. Circuits Syst. I Regul. Pap.* **2013**, *60*, 867–874. [CrossRef]
24. Lim, Y.; Tang, H.; Lim, S.; Park, J. An Adaptive Impedance-Matching Network Based on a Novel Capacitor Matrix for Wireless Power Transfer. *IEEE Trans. Power Electron.* **2014**, *29*, 4403–4413. [CrossRef]
25. Lee, G.; Waters, B.H.; Shin, Y.G.; Smith, J.R.; Park, W.S. A Reconfigurable Resonant Coil for Range Adaptation Wireless Power Transfer. *IEEE Trans. Microw. Theory Tech.* **2016**, *64*, 624–632. [CrossRef]
26. Fu, M.; Ma, C.; Zhu, X. A Cascaded Boost–Buck Converter for High-Efficiency Wireless Power Transfer Systems. *IEEE Trans. Ind. Inform.* **2014**, *10*, 1972–1980. [CrossRef]
27. Li, H.; Li, J.; Wang, K.; Chen, W.; Yang, X. A Maximum Efficiency Point Tracking Control Scheme for Wireless Power Transfer Systems Using Magnetic Resonant Coupling. *IEEE Trans. Power Electron.* **2015**, *30*, 3998–4008. [CrossRef]
28. Dai, X.; Li, X.; Li, Y.; Hu, A.P. Maximum Efficiency Tracking for Wireless Power Transfer Systems with Dynamic Coupling Coefficient Estimation. *IEEE Trans. Power Electron.* **2018**, *33*, 5005–5015. [CrossRef]
29. Zhong, W.X.; Hui, S.Y.R. Maximum Energy Efficiency Tracking for Wireless Power Transfer Systems. *IEEE Trans. Power Electron.* **2015**, *30*, 4025–4034. [CrossRef]
30. Zhong, W.; Hui, S.Y.R. Charging Time Control of Wireless Power Transfer Systems Without Using Mutual Coupling Information and Wireless Communication System. *IEEE Trans. Ind. Electron.* **2017**, *64*, 228–235. [CrossRef]
31. Nayak, J.; Swapnarekha, H.; Naik, B.; Dhiman, G.; Vimal, S. 25 Years of Particle Swarm Optimization: Flourishing Voyage of Two Decades. *Arch. Comput. Methods Eng.* **2023**, *30*, 1663–1725. [CrossRef]
32. Zhao, S.; Blaabjerg, F.; Wang, H. An Overview of Artificial Intelligence Applications for Power Electronics. *IEEE Trans. Power Electron.* **2021**, *36*, 4633–4658. [CrossRef]